



LAWRENCE  
LIVERMORE  
NATIONAL  
LABORATORY

# General Model of Conversion Efficiency in Ultraintense Laser-Overdense Plasma Interactions

M. C. Levy, S. C. Wilks, M. Tabak, M. G. Baring

June 21, 2013

Physics of Plasmas

## **Disclaimer**

---

This document was prepared as an account of work sponsored by an agency of the United States government. Neither the United States government nor Lawrence Livermore National Security, LLC, nor any of their employees makes any warranty, expressed or implied, or assumes any legal liability or responsibility for the accuracy, completeness, or usefulness of any information, apparatus, product, or process disclosed, or represents that its use would not infringe privately owned rights. Reference herein to any specific commercial product, process, or service by trade name, trademark, manufacturer, or otherwise does not necessarily constitute or imply its endorsement, recommendation, or favoring by the United States government or Lawrence Livermore National Security, LLC. The views and opinions of authors expressed herein do not necessarily state or reflect those of the United States government or Lawrence Livermore National Security, LLC, and shall not be used for advertising or product endorsement purposes.

# General Model of Conversion Efficiency in Ultraintense Laser-Overdense Plasma Interactions

Matthew C. Levy,<sup>1,2</sup> Scott C. Wilks,<sup>2</sup> Max Tabak,<sup>2</sup> and Matthew G. Baring<sup>1</sup>

*<sup>1</sup>Department of Physics and Astronomy, MS  
108, Rice University, Houston, Texas 77005, USA*

*<sup>2</sup>Lawrence Livermore National Laboratory, Livermore, California 94551, USA\**

(Dated: June 12, 2013)

## Abstract

Particle coupling to the oscillatory and steady-state nonlinear force of an ultraintense laser is studied through analytic modeling and particle-in-cell simulations. The complex interplay between these absorption mechanisms – corresponding respectively to ‘hot’ electrons and ‘hole punching’ ions – is central to the viability of many ultraintense laser applications. Yet, analytic work to date has focused only on limiting cases of this key problem. In this paper, we develop a fully-relativistic model in 1-D treating both modes of ponderomotive light absorption on equitable theoretical footing for the first time. Using this framework, analytic expressions for the conversion efficiencies into hole punching ions and into hot electrons are derived. Self-consistent solutions for the relativistically-correct hole punching velocity and the hot electron Lorentz factor are also calculated. Excellent agreement between analytic predictions and particle-in-cell simulations is demonstrated, and astrophysical analogies are highlighted.

---

\*Electronic address: [levy11@llnl.gov](mailto:levy11@llnl.gov)

## I. INTRODUCTION

The interaction of ultraintense laser light (normalized vector potential  $a_0 = eE_L/(m_e c \omega_L) > 1$ ) with matter is characterized by the nonlinear action of the light[1]. The laser ponderomotive force  $f_L$  couples the incident photon flux into two primary kinetic modes: (1) 'hole boring' or 'hole punching' (hp) ions accelerated by the space-charge force associated with electrons under the excursion of time-averaged field energy gradients  $\langle f_L \rangle \sim \nabla E_L^2$ ; and (2) relativistic 'hot' electrons excited by the oscillatory component of  $f_L$  at  $2\omega_L$ . Optimizing the modes in which the photons are absorbed enables applications such as compact GeV-scale particle accelerators[2], approaches to inertial confinement fusion[3] (ICF), and medical proton oncology[4].

The complex interplay between the steady-state and oscillatory ponderomotive absorption processes is central to the viability of many ultraintense laser applications. Yet, to date, analytic models seeking to describe the interaction have only considered only limiting cases, e.g., assuming unitary coupling into either the steady-state hole punching (hp) absorption mode[1] or into the oscillatory mode[5].

In this paper, we develop a fully-relativistic 1-D analytic model treating both modes of ponderomotive light absorption on equitable theoretical footing for the first time. Using this framework, we derive analytic solutions for the (1) piston velocity, (2) hole punching ion velocity, (3) hot electron Lorentz factor, (4) conversion efficiency into hole punching ions, and (5) conversion efficiency into hot electrons. The model describes overdense plasma interactions and is insensitive to laser polarization assuming that bulk ions are swept up and fully reflected in the interaction. Excellent agreement between analytic predictions and particle-in-cell simulations is demonstrated.

The kinematic approach undertaken here considers the distribution functions  $f_s$  describing the exchange-mediating particles, i.e. those directly excited by the laser on the spatial scale  $c/\omega_{pe}$  at the laser-plasma (LP) interface. The set  $s$  fully enumerates these populations,  $s \in \{\text{hole punching ions, hole punching electrons, hot electrons}\}$ ; once the laser has coupled into these particles, energy and momentum may then cascade into other species in the plasma, e.g. drawing the return current[5] or generating positrons[6]. Now, in momentum space,  $f_s = f_s(p^k; \langle p_s^0 \rangle)$  where  $\langle p_s^0 \rangle = \int p^0 f_s dp^k$  (covariant notation is discussed in section III). The task is thus to determine  $\langle p_s^0 \rangle$  such that energy and momentum are

conserved between the plasma and the laser driver.

This paper is structured as follows: section II provides a brief review of existing analytic absorption models. In section III, an overview of the approach undertaken here is discussed, and sections IV and V establish the foundations of the model. Section VI calculates the solutions for  $\langle p_s^0 \rangle$ , and section VII derives the conversion efficiencies into hole punching ions and into hot electrons. In section VIII, the analytic results are compared to particle-in-cell simulations. Finally, section IX discusses important analogies to astrophysical scenarios, and concluding remarks are given in section X.

## II. BACKGROUND

The task of understanding the critical interface exchange processes for  $a_0 > 1$  LPI amounts to understanding the partitioning of the laser energy and momentum into hot electrons and hole punching ions. Yet, to date, a general framework treating both populations on equitable theoretical footing has not been developed. The model of momentum conservation between an ultraintense laser and an overdense plasma was described by Wilks *et al.*[1], which derived the hole punching velocity by balancing the laser momentum flux with that of the hole punching ions. Yet, in this model the hot electrons were not accounted for, nor was energy conservation considered. Naumova *et al.*[7] extended this framework for relativistic hole punching ions and taking into account energy flux conservation.

This work considered full laser light reflection from the electron density peak bounding the radiation pressure-induced separation layer at the critical interface. In this context, the energy transferred to the plasma is that which is lost in the red-shifting of the reflected light, with an effective reflection coefficient[7] given by the relativistic doppler formula  $\mathcal{R} = (1 - u_p/c)/(1 + u_p/c)$ . This energy is assumed to be coupled with 100% efficiency into the punching ions. In the nonrelativistic limit, the energy absorbed by the ions is then simply  $1 - \mathcal{R} \simeq 2u_p/c$ , consistent with the simple estimate of Wilks & Kruer[8]. To the extent the laser piston structure is maintained with unit coupling into ions, recent measurements of the specular doppler shift[9] represent a 1 : 1 measurement of the ion conversion efficiency.

In considering the fast electrons, Haines *et al.*[5] developed a 'black box' model conserving both energy and momentum in the interaction, in a manner analogous to the Rankine-Hugoniot shock relations. Yet, this model took into account only the contributions from the

hot electrons. More recently, Ping *et al.*[9] put forward a model that includes both the hot electron and hole punching ions; however, this model is constrained to the limit where the hole punching ions exchange momentum but not energy with the laser.

In the following sections, we present a novel analytic model extending this framework by allowing energetically significant absorption into both the steady-state and oscillatory modes for the first time. In Section VIII, results from the model are compared to and shown to be in good agreement with particle-in-cell simulations.

### III. COUPLING OF ULTRAIINTENSE LASER LIGHT TO AN OVERDENSE PLASMA

We consider the *steady-state* laser-plasma interaction *at the coupling stage* in the *laboratory frame*. Consider the small volume at the laser-plasma interface comprising a few  $c/\omega_{pe}$  in a axial extent, depicted schematically in Fig. 1. The laser is incident on the volume from the left and excites plasma particles which leave the volume on the right-hand side. All particles in the region are assumed to interact with the laser and may be accelerated relativistically by coupling into either the oscillatory or steady-state absorption mode. The total electron density is  $n_e$ , which may take on any value that is relativistically-opaque to the laser light[10]. Ions in the interface are assumed to have uniform charge state  $Z$  given by the quasi-neutrality condition,  $n_i = n_e/Z$ .

Absorption of ultraintense laser light by an overdense plasma amounts, in effect, to the coupling between an incident photon flux and particles comprising the moving plasma interface. It follows that we consider *only* plasma particles that mediate the energy and momentum exchange, i.e. those directly excited by the laser on the spatial scale  $c/\omega_{pe}$  at the laser-plasma (LP) interface. The set  $s$  fully enumerates these populations,

$$s \in \{\text{hp ions, hp electrons, hot electrons}\} \quad (1)$$

where in the following sections each species will be referred to by its numeric index. Once the laser has coupled into these populations, energy and momentum may then cascade into other species in the plasma. An important example of this is the collective plasma excitation of a return current in order to neutralize the fast electron current[5].

The evolution of particle distribution functions  $f_s(x^\mu, p^\mu)$  in equation (1) is determined

by the Boltzmann-Vlasov equation,

$$\left( \frac{dx^\mu}{d\tau} \frac{\partial}{\partial x^\mu} + \frac{dp^k}{d\tau} \frac{\partial}{\partial p^k} \right) f_s(x^\mu, p^\mu) = 0 \quad (2)$$

where  $\tau$  is the proper time[11]. The Minkowski tensor  $\eta^{\mu\nu}$  has signature  $(-1, 1, 1, 1)$ ; the greek sub- and super-scripts represent tensor indices  $\mu \in \{0, 1, 2, 3\}$ ; the latin indices  $k \in \{1, 2, 3\}$  run over the spatial subset; the  $s$  subscript is reserved for particle species and for clarity will be distinguished from tensor indices where necessary. Collisional coupling is assumed to be negligible and the characteristics of equation (2) are given by,

$$\frac{dx^\mu}{d\tau} = \frac{p^\mu}{m_s}, \quad \frac{dp^k}{d\tau} = -\frac{q_s}{m_s} F^{k\mu} p_\mu \quad (3)$$

where the momentum characteristic includes spatial components due to the mass-shell restriction[11]. In equations (2) and (3),  $q_s$  is the electric charge,  $m_s$  is the rest mass and  $F^{\mu\nu}$  represents the field strength tensors.

The approach undertaken in this paper considers the parameters of  $f_s$  that satisfy conservation of energy and momentum between the ultraintense photon flux and relativistic particle fluxes excited in the plasma, e.g. moments of equation (2). In momentum space,  $f_s = f_s(p^k; \langle p_s^0 \rangle)$  where  $\langle p_s^0 \rangle = \int p^0 f_s dp^k$ . We thus seek to determine  $\langle p_s^0 \rangle$  for the hp particles and hot electrons.

For the former population, we note that the 'laser piston'[7] is characterized by the strong electrostatic potential generated by the steady-state component of the laser ponderomotive force[12],

$$\mathbf{f}_L = \nabla \left( \frac{n_{cr}}{n_e} a_0^2 \right) m_e c^2 \quad (4)$$

where  $n_e$  is the electron density in the laser-plasma interface. As the piston propagates into the target, we assume that background particles are swept up and fully reflected[1, 7, 13, 14]. Electrons reflect from the piston head while ions are pulled in by the potential and reflect from ions bounding the piston on the downstream side. Electrons and ions are both reflected at the same velocity,  $u_i$ . As such, we assume they are adequately represented in momentum space as drifting Maxwellian distributions of the same form,

$$f_{s_n}(v) = \frac{n_n}{\sqrt{2\pi}} \sqrt{\frac{m_n}{T_n}} e^{-\frac{m_n(v-u_i)^2}{2T_n}}, \quad n \in \{1, 2\} \quad (5)$$

where, related to equation (1),  $f_{s_1}$  represents the hole punching ion distribution and  $f_{s_2}$  represents the hole punching electron distribution.  $m_n$  is the mass,  $n_n$  is the reflected

particle density and  $T_n$  is the temperature of population  $s_n$ . The strong light pressure driving the piston through equation (4) can accelerate the particles to 'mildly' relativistic energies with  $u_i/c \sim 0.1$ . We assume that each distribution is cold so that  $1/2m_n u_i^2 \gg T_n$ , consistent with the particle-in-cell simulation results. More accurately, however, the 'saddle point' approximation of the Juttner distribution should be employed[15].

If the phase offset  $\Delta\phi$  between the laser electric field components is not precisely  $\pi/2$ ,  $\mathbf{f}_L$  also contains an oscillatory term that nonadiabatically accelerates 'strongly' relativistic electrons[12]. These 'hot' electrons are well-characterized by a Maxwell-Juttner distribution,

$$f_{s_3}(\gamma) = \frac{n_h}{\Theta} \frac{\gamma^2 \sqrt{1 - \gamma^{-2}}}{K_2(1/\Theta)} e^{-\gamma/\Theta} \quad (6)$$

where  $n_h$  is the hot electron density,  $\gamma$  is the Lorentz factor,  $\Theta = T_h/(m_e c^2)$ ,  $T_h$  is the temperature and  $K_2$  is the modified Bessel function of the second kind.

In the following sections we seek to determine the parameters  $\langle p_s^0 \rangle$  of  $f_s$  that satisfy energy and momentum conservation between the ultraintense laser and plasma.

#### IV. RELATION BETWEEN THE PISTON AND HOLE PUNCHING VELOCITIES

In a time-averaged sense, ultraintense LPI at the critical density  $n_{cr} = m_e \omega_L^2 / (4\pi e^2)$  interface are characterized by the generation of a radiation pressure separation layer, comprised of electrons swept out by the laser fields, resulting in regions of charge compression and depletion. Ions are pulled along through the generation of a strong ambipolar force field, with the entire 'laser piston' structure propagating into the bulk target at the piston velocity  $u_p$ . Particle mass density is conserved as the piston sweeps up and reflects background electrons and ions. From this, the relation between the piston velocity  $u_p$  and reflected ion velocity  $u_i$  can be obtained.

By integrating over equation (2) the continuity equation is obtained,

$$\frac{\partial \Gamma_s^\mu}{\partial x^\mu} = 0, \quad \Gamma_s^\mu = \frac{n'_s}{m_s} P_s^\mu \quad (7)$$

where  $n'_s$  is the Lorentz-invariant proper density of species  $s$ [11]. The fluid four-momentum  $P_s^\mu = \gamma_s m_s c (1, \mathbf{V}_s/c)$  is defined as,

$$P_s^\mu = \frac{1}{n_s} \int p^\mu f_s dp^k \quad (8)$$

where the Lorentz factor  $\gamma_s = (1 - \mathbf{V}_s \cdot \mathbf{V}_s/c^2)^{-1/2}$ . The particle density  $n_s$  is given by,

$$n_s = \int f_s dp^k \quad (9)$$

For a frame moving at velocity  $u$  relative to  $V_s$ , invariance of electric charge and equation (7) give the relation,  $n_s = \gamma(u) n'_s$  where  $\gamma(u) = (1 - u^2/c^2)^{-1/2}$ .

We evaluate equation (7) by changing coordinates to the rest frame of the piston. Quantities in this frame are denoted using a superscript  $(p)$ . For the laboratory frame velocity  $u$ , the appropriate Lorentz transformation is given by,

$$u^{(p)} = \frac{u - u_p}{1 - u \cdot u_p/c^2} \quad (10)$$

In this frame, the interaction is steady-state and longitudinal particle conservation may be expressed,

$$-Mn_i u_p + Mn_i u_i^{(p)} = 0 \quad (11)$$

where  $n_i$  is the ion density in the laser-plasma interface,  $u_p$  is the piston velocity and  $u_i^{(p)}$  is the axial velocity of the reflected ions in the piston frame. Note that equation (11) represents particle conservation for both the hole punching electrons and ions, as  $M = M_i + Zm_e$ .

From equation (11) it follows immediately that  $u_i^{(p)} = u_p$ . Transforming back to the laboratory frame gives the hole punching ion axial velocity,

$$u_i = \frac{2u_p}{1 + (u_p/c)^2} \quad (12)$$

consistent with Wilks *et al.*[1] in the nonrelativistic limit.

We now introduce the relativistic 'hot' electron beam into this framework. This is possible due to the separation of velocity scales associated with the oscillatory and steady-state components of the nonlinear force. As was suggested by Ping *et al.*[9], the plasma return current neutralizes the electron beam at a rate much faster than the piston velocity, i.e.  $u_h/u_p \gg 1$  where  $u_h \simeq c$  is the hot electron axial velocity. The interaction is thus steady-state on the piston timescale, such that the electron density as 'seen' by the piston is unmodified. Particle number conservation for the hot electrons may then be written,

$$m_e n_e u_r + m_e n_h u_h = 0 \quad (13)$$

where  $u_r = -(n_h/n_e)u_h$  is the return current velocity, i.e. a statement of the plasma neutralization of the hot electron beam current. The interplay between the laser light and the plasma near the critical interface is illustrated schematically in Fig. 1.

In the framework of the usual two-temperature fit to the electron  $dN/dE$  energy spectrum[8], the steady-state nonlinear force may be considered as corresponding to the low-energy component of the electron spectrum, and the oscillatory component as corresponding to the high-energy component. While the hot electrons may play a significant role energetically due to their relativistic  $\gamma$ -factor, in general it is expected that  $n_h/n_e \ll 1$ , as inspection of the electron energy spectrum from a typical experiment or simulation shows that the majority of the *number of electrons* in the system fall into the lower-energy component.

## V. POYNTING THEOREM FOR ULTRAINTENSE LIGHT

Once the laser has excited populations  $s$ , their evolution is determined through conservation of phase volume given by equation (2). The parameters  $\langle p_s^0 \rangle$  of  $f_s$  are determined by the four-divergence of the electromagnetic stress-energy tensor  $T^{\mu\nu}$ ,

$$\frac{\partial T^{\mu\nu}}{\partial x^\nu} + \eta^{\mu k} \frac{dp_k}{d\tau} = 0 \quad (14)$$

where the characteristic is given in equation (3) and the stress-energy tensor is,

$$T^{\mu\nu} = \frac{1}{4\pi} \left( F^{\mu\alpha} F_\alpha^\nu - \frac{1}{4} \eta^{\mu\nu} F_{\alpha\sigma} F^{\alpha\sigma} \right) \quad (15)$$

where  $\eta^{\mu\nu}$  is the metric tensor and  $F^{\mu\nu}$  is the field strength tensor as above.

In this section, we will evaluate the four conservation laws implied by equation (14) in Euclidean space. This approach allows us to highlight effects related to the relativistic particle fluxes central to ultraintense laser-plasma interactions.

Consider the electromagnetic energy density  $U_e$  in the box shown in Fig. 1. The Poynting theorem stipulates that,

$$-\frac{\partial U_e}{\partial t} = \nabla \cdot \mathbf{S}_e + \sum_s \mathbf{J}_s \cdot \mathbf{E} \quad (16)$$

where  $\mathbf{S}_e$  is the electromagnetic Poynting flux and  $\mathbf{J}_s$  is the spatial component of the current four-vector,

$$J_s^\mu = \frac{q_s n'_s}{m_s} P_s^\mu \quad (17)$$

and  $P_s^\mu$  is given by equation (8).

As the light becomes ultraintense, the kinetic energy associated with the relativistic particle flux becomes significant. To elucidate this effect, the term in equation (16) corresponding to the work done against the Lorentz force can be written as,

$$\sum_s \mathbf{J}_s \cdot \mathbf{E} = \frac{\partial U_m}{\partial t} + \nabla \cdot \mathbf{S}_m \quad (18)$$

where  $U_m$  is the 'mechanical' energy density in the box.  $\mathbf{S}_m$  is the mechanical Poynting vector corresponding to a sum over the particle energy flux density,

$$\mathbf{S}_m = \sum_s \frac{P_s^k}{\gamma_s m_s} (P_s^0 c - m_s c^2) n_s \quad (19)$$

A form of Poynting's theorem useful to ultraintense laser interactions is obtained by substituting equations (18-19) into (16),

$$\frac{\partial U}{\partial t} + \nabla \cdot (\mathbf{S}_e + \mathbf{S}_m) = 0 \quad (20)$$

where  $U = U_e + U_m$  is the total energy density in the region. Equation (20) states that in a steady-state interaction for the region in Fig. 1, the sink in the electromagnetic Poynting flux must be balanced by a source of kinetic particle flux.

It is straight forward to derive an analogous conservation law for the vector momentum flux density,

$$\frac{\partial \mathbf{p}}{\partial t} + \nabla \cdot (\mathfrak{P}_e + \mathfrak{P}_m) = 0 \quad (21)$$

where  $\mathfrak{P}_e$  and  $\mathfrak{P}_m$  are second rank tensors describing the flow of electromagnetic and mechanical momentum flux, and  $\mathbf{p}$  is the total momentum density in the box in Fig. 1.

We conclude this section by commenting on the dynamical nature of the laser-plasma interface. The fact the interface is in motion in the laboratory frame plays an important role in satisfying equations (20-21). In general, an electromagnetic flux through a surface moving at velocity  $u_p$  becomes,

$$\mathbf{S}_e \rightarrow \left(1 - \frac{u_p}{c}\right) \mathbf{S}_e \quad , \quad \mathfrak{P}_e \rightarrow \left(1 - \frac{u_p}{c}\right) \mathfrak{P}_e \quad (22)$$

In the next section, these conservation laws will be applied to determine the properties of  $f_s$  for the exchange-mediating particle populations in equation (1).

## VI. FULLY-RELATIVISTIC MODEL OF ULTRAINTENSE LASER LIGHT ABSORPTION

Using the tools in the preceding sections, we now develop a model of ultraintense laser light absorption by an overdense plasma. For the first time, both hot electrons and hole punching particles are described relativistically and exchange both energy and momentum with the laser.

We consider the *steady-state* laser-plasma interaction *at the coupling stage* in the *laboratory frame*. The ensemble average momentum and kinetic energy for each population excited by the laser are given by,

$$\langle \mathbf{p}_s \rangle = P_s^k \quad (23)$$

$$\langle \mathcal{E}_s \rangle = P_s^0 c - m_s c^2 \quad (24)$$

The brackets are employed to emphasize that equations (23-24) represent ensemble average quantities.

Over time interval  $dt$ , the total energy and momentum coupled by the laser into the particles in equation (1) is simply,

$$\begin{aligned} d\mathcal{E}_s &= N_s d\langle \mathcal{E}_s \rangle + \langle \mathcal{E}_s \rangle dN_s \\ d\mathbf{p}_s &= N_s d\langle \mathbf{p}_s \rangle + \langle \mathbf{p}_s \rangle dN_s \end{aligned} \quad (25)$$

where  $N_s$  is the particle number and ergodicity implies that  $d\langle \mathcal{E}_s \rangle$  and  $d\langle \mathbf{p}_s \rangle$  are zero.

The number of ions accelerated by the laser piston over  $dt$  is,

$$dN_{s_1} = n_i u_p dA dt \quad (26)$$

where  $dA = 2\pi r dr$  for a uniform laser spot of radius  $r$ . As in previous sections,  $n_i$  is the ion density in the interface and  $u_p$  is the piston velocity. By equation (11), the number of hole punching electrons excited over  $dt$  is  $dN_{s_2} = [Z \times \text{equation (26)}]$ .

The ensemble average particle energy and momentum can be related to the laser-plasma kinematic exchange using equations (5, 19-21, 23-26). The 1-D momentum and energy flux associated with the hole punching particles can be calculated as,

$$\begin{aligned} \mathcal{P}_{s_n} &= \frac{dp_n}{dA dt} = \langle p_n \rangle u_p n_n \\ \mathcal{F}_{s_n} &= \frac{d\mathcal{E}_n}{dA dt} = \langle \mathcal{E}_n \rangle u_p n_n \quad , \quad n \in \{1, 2\} \end{aligned} \quad (27)$$

where  $\mathcal{P}_{s_n}$  ( $\mathcal{F}_{s_n}$ ) is the momentum (energy) flux. As in the previous sections,  $n_{s_1} = n_i$ ,  $n_{s_2} = Zn_i$ .

On the other hand, the number of hot electrons  $dN_{s_3}$  excited by the oscillatory component of the laser over  $dt$  is not directly related to the piston dynamics. As noted in equation (13), particle number is conserved in the interaction with the plasma return current on a timescale fast compared to  $u_p$ . From equations (6) and (23-24) we can assume that the hot electron momentum and energy flux densities are given by,

$$\mathcal{P}_{s_3} = \gamma_h n_h m_e u_h^2, \quad \mathcal{F}_{s_3} = (\gamma_h - 1) u_h n_h m_e c^2 \quad (28)$$

where  $u_h \simeq c$  is the hot electron axial velocity. In contrast to  $n_{s_1}$  and  $n_{s_2}$ ,  $n_h$  is an ansatz for the hot electron density. In taking the kinematic form of equation (28), no assumptions are made with respect to the hot electron dynamical motion[5].  $\gamma_h$  corresponds to the ensemble average hot electron Lorentz factor; brackets have been omitted for simplicity of notation.

Equations (27-28) constitute the mechanical Poynting flux  $\mathbf{S}_m$  in equation (20). Integrating over the volume of the box in Fig. 1 and invoking the Divergence theorem gives,

$$\frac{1}{A_b} \int \int \mathbf{S}_m \cdot d\mathbf{A}_b = - \sum_s \mathcal{F}_s \quad (29)$$

as the particle flux leaves the region on the right side. Here  $\mathbf{A}_b$  is the area of the surface bounding the box, with vector direction normal to the surface.

Noting equation (22), the laser Poynting flux in equation (20) in integral form can be written,

$$\frac{1}{A_b} \int \int \mathbf{S}_e \cdot d\mathbf{A}_b = \left(1 - \frac{u_p}{c}\right) (1 - \mathcal{R}) I_L \quad (30)$$

where  $I_L$  is the laser intensity reaching the overdense surface and  $\mathcal{R}$  is the fraction of reflected irradiance. Using equations (29) and (30), the fully-relativistic energy flux conservation equation can be expressed,

$$(1 - \mathcal{R}) (1 - \beta_p) I_L = (\gamma_h - 1) m_e n_h c^3 + (\gamma_i - 1) M n_i \beta_p c^3 \quad (31)$$

where  $M = M_i + Zn_e$  as in the preceding sections,  $\beta_p = u_p/c$  is the dimensionless piston velocity,  $u_i$  is given by equation (12) and  $\gamma_i = (1 + \beta_p^2)/(1 - \beta_p^2)$ . The first term on the right-hand side of equation (31) represents coupling of the ultraintense laser light into the oscillatory mode of the nonlinear force, and the second term corresponds to coupling into the

steady-state mode, the kinetic manifestation of which is the bulk electrons and ions reflected from the piston. The fast electron current neutralization described by  $[(e/m_e) \times \text{equation (13)}]$  represents a collective response of the plasma to the beam. As noted above, the energy driving the return current is extracted from the beam itself and thus does not factor into the coupling equations.

Similarly, momentum flux conservation from equation (21) can be expressed,

$$(1 + \mathcal{R}) (1 - \beta_p) \frac{I_L}{c} = \gamma_h m_e n_h c^2 + \gamma_i \beta_p M n_i u_i c \quad (32)$$

where equations (27) and (28) have been used.

Full reflection of background particles implies that the radiation pressure layer remains essentially depleted of electrons. It is thus clear that the fast electrons must be primarily generated at supercritical densities and may be shielded by the bulk target electrons from the full ponderomotive potential. As such, it is emphasized that  $\gamma_h$  does not *a priori* follow the ponderomotive scaling[1], i.e.  $\gamma_h \neq (1 + a_0^2)^{1/2}$ , but rather may be self-consistently determined through equations (32-31).

Employing the relation  $2I_L/c = m_e n_{cr} a_0^2 c^2$ , equations (32) and (31) may be reformulated as,

$$(1 - \beta_p) (1 + \mathcal{R}) = \frac{\gamma_h m_e n_h}{\beta_0^2 M n_i} + \frac{1}{\beta_0^2} \frac{2\beta_p^2}{1 - \beta_p^2} \quad (33)$$

$$(1 - \beta_p) (1 - \mathcal{R}) = \frac{(\gamma_h - 1) m_e n_h}{\beta_0^2 M n_i} + \frac{\beta_p}{\beta_0^2} \left( \frac{1 + \beta_p^2}{1 - \beta_p^2} - 1 \right) \quad (34)$$

where  $\beta_0$  is the dimensionless shock velocity scale,

$$\beta_0 = \left( \frac{I_L}{n_i M_i c^3} \right)^{1/2} = \left( \frac{Z m_e n_{cr}}{2 M_i n_e} \right)^{1/2} a_0 \quad (35)$$

As  $\beta_0$  becomes closer to unity, it no longer closely approximates the actual piston velocity  $\beta_p$ . For simplicity of notation, we adopt the convention that linear light with normalized potential  $a_0$  has identical energy density to circular light of  $a_0/\sqrt{2}$ .

$\{\gamma_h, \beta_p\}$  parameterize  $f_s$  and thus determine the LP equilibrium condition. Problematically, however, equations (34-33) make evident the additional degree of freedom associated with the hot electrons,  $n_h$ . We treat this by defining,

$$\bar{\rho}_h \equiv \frac{\rho_h}{\sum \rho} = \frac{Z m_e n_h}{M n_e} \quad (36)$$

where  $\bar{\rho}_h$  represents the *relative mass density* in the interaction region coupled into the oscillatory mode. While the electrons may play a significant role energetically due to the relativistic  $\gamma$ -factor, equation (36) shows that  $\bar{\rho}_h \ll 1$ , as the maximum value of  $\bar{\rho}_h \sim Zm_e/M$  as  $n_h/n_e \sim 1$ .

Solutions to equations (33-34) can now be obtained using a series expansion. To zeroth order in  $\bar{\rho}_h$ ,

$$\beta_p = \beta_0 \left( \frac{\mathcal{R}}{1 + \mathcal{R}\beta_0^2} \right)^{1/2} \quad (37)$$

Equation (37) represents the fully-relativistic hole punching velocity, taking into account both oscillatory hot electron generation and steady-state acceleration of background particles by the laser piston. This expression is valid for overdense laser-plasma interactions while background ions are fully-reflected by the laser light, independent of the laser polarization and fraction of reflected light  $\mathcal{R}$ . The parametric instabilities associated with relativistic light interacting with an underdense plasma represent additional vectors through which the light may couple to the plasma, and have been shown to lead to the formation of a supraponderomotive tail in the electron spectrum[16]. In effect, this would increase the number of exchange-mediating populations in equation (1), e.g. Raman-scattering electrons[8].

Equation (37) is independent of  $\bar{\rho}_h$ , showing that the interplay between the piston velocity  $\beta_p$  and light coupled into the oscillatory mode is indirect, occurring only as the fast electron absorption increases the total light absorbed by the plasma. Equation (37) also predicts a decrease in piston velocity as total absorption increases, with  $\beta_p \rightarrow 0$  as  $\mathcal{R} \rightarrow 0$ . This limit corresponds to the cases described by Haines *et al.*[5] and Ping *et al.*[9].

The piston velocity from Wilks *et al.*[1],  $\sqrt{(1 + \mathcal{R})/2} \beta_0$ , can be derived exactly from equation (32) in the limits that  $n_h \rightarrow 0$  and  $\beta_0 \ll 1$ . This expression is close to our result for  $\beta_p$  in the nonrelativistic limit, but diverges as  $\beta_p \gtrsim 0.1$ . It is straight-forward to show that the relativistically-correct piston velocity for 100% conversion efficiency into ions as found by Naumova *et al.*[7],  $u_p/c = \beta_0/(1 + \beta_0)$ , represents a contour along the surface defined by equation (37). Indeed, this result follows exactly from our equations (32) and (31) in the limit  $n_h \rightarrow 0$ . It should also be noted that equation (37) reduces in the nonrelativistic ion limit to  $\sqrt{\mathcal{R}} \beta_0$ , equivalent to the expression found in [9] for linearly-polarized light, despite quite distinct assumptions in the underlying model.

From equations (33-34) and (37), we find that the solution for  $\gamma_h$  contains two terms to

zeroth order in  $\bar{\rho}_h$ ,

$$\gamma_h = \frac{(1 - \mathcal{R})\sqrt{\beta_0^2 \mathcal{R} + 1} - \beta_0 \sqrt{\mathcal{R}}(1 + \mathcal{R})}{\sqrt{\beta_0^2 \mathcal{R} + 1} \beta_0^{-2}} \bar{\rho}_h^{-1} + O(1) \quad (38)$$

The  $O(1)$  term is a polynomial in  $\beta_0$  and  $\mathcal{R}$ . Fig. 2 shows the contours of the  $O(1)$  term. Fig. 3 depicts the solutions  $\{\gamma_h, \beta_p\}$  from equations (37) and (38). The ensemble average hot electron energy  $\gamma_h$  scales as  $\sim \bar{\rho}_h^{-1}$ , while from equation (31) the total energy coupled into the oscillatory mode  $\sim \gamma_h \bar{\rho}_h$  is independent of the parameter. This will be discussed in more detail in Section VII.

With the piston velocity  $\beta_p$  in equation (37) and the ensemble average hot electron energy  $\gamma_h$  in equation (38), the distribution functions  $f_s$  in equation (1) are fully-characterized. Together with equation (12) relating  $u_i$  to the piston velocity, these equations satisfy energy and momentum conservation between an ultraintense laser and overdense plasma.

In the next sections, we will examine how these analytic solutions change as system parameters, e.g. the total reflection  $\mathcal{R}$ , vary and are subject to constraints. We will show that knowing the properties of  $f_s$  allows us to extract information about the global properties of the system.

## VII. CONVERSION EFFICIENCY INTO HOT ELECTRONS AND HOLE PUNCHING IONS

Finally, let us consider the conversion efficiency of laser light into populations listed in equation (1).

From equations (34) and (37) we can calculate the conversion efficiency into hot electrons,

$$f_a^h = (\gamma_h - 1) \bar{\rho}_h \frac{\beta_0^{-2}}{1 - \beta_0 \sqrt{\frac{\mathcal{R}}{\beta_0^2 \mathcal{R} + 1}}} \quad (39)$$

Using equation (38), this expression can be expanded as,

$$f_a^h = \frac{(1 - \mathcal{R})\sqrt{\beta_0^2 \mathcal{R} + 1} - (1 + \mathcal{R})\beta_0 \sqrt{\mathcal{R}}}{\sqrt{\beta_0^2 \mathcal{R} + 1} - \beta_0 \sqrt{\mathcal{R}}} + O\left(\frac{\bar{\rho}_h}{\beta_0^2}\right) \quad (40)$$

Equation (40) illustrates the key result that while the per-electron energy depends on  $\bar{\rho}_h$  through  $\gamma_h \simeq 1 + (\bar{\rho}_h^{-1})$ , the total energy coupled into electrons  $f_a^h$  depends only on  $\beta_0$  and  $\mathcal{R}$  while  $\bar{\rho}_h/\beta_0^2 \gtrsim 1$ .

For the laser conversion efficiency into hole punching ions,  $f_a^p$ , we have,

$$f_a^p = \frac{2\beta_0\mathcal{R}^{3/2}}{\sqrt{\beta_0^2\mathcal{R} + 1} - \beta_0\sqrt{\mathcal{R}}} \quad (41)$$

As for  $f_a^h$ , we observe that the conversion efficiency into hole punching ions is robust to the hot electron mass density  $\bar{\rho}_h$ . The conversion efficiencies from equations (40) and (41) highlight the nonlinear dependency of the coupling on the shock velocity scale  $\beta_0$  and the total light absorption  $1 - \mathcal{R}$ . The solutions for the conversion efficiencies are depicted in Fig. 3.

In the following section we will compare the predictions of equations (40) and (41) to particle-in-cell simulations.

### VIII. PARTICLE-IN-CELL SIMULATIONS

To test the predictions of the analytic model we have performed PIC simulations using the hybrid LSP code[17]. The code is configured to solve the discretized Maxwell's equations and Lorentz force equation implicitly, with no time biasing to avoid numerical damping of light waves. The timestep is determined by the Courant condition multiplied by a factor of 0.1. Electrons and ions are fully kinetic and are represented using 500 particles/cell/species. We have modified the LSP source code to implement a 'kinetic-to-kinetic' particle migration feature. This allows us to effectively distinguish, label and track electrons which interact with the laser and exceed a kinetic energy threshold from the cold background.

Simulations are one-dimensional Cartesian geometry with uniform spatial resolution  $(\Delta x)^{-1} = 16$  cells/ $\mu\text{m}$ . Laser light enters the box at the left  $x = 0$  boundary and is incident upon an overdense  $Z/A = 1$  plasma slab at  $x = 5\mu\text{m}$ . The slab density ramps to peak density  $n_0 = n_e = Zn_i$  over  $0.06\mu\text{m}$  and has a  $290\mu\text{m}$  spatial extent, followed by  $5\mu\text{m}$  of vacuum ahead of the right boundary; the box is effectively infinite to prevent electron refluxing. The laser pulse has  $1\mu\text{m}$  wavelength and rises over 3 optical cycles to a flat-top profile with 500-700fs duration. The plasma density  $n_0$  and normalized laser amplitude  $a_0$  are varied across simulations.

We exploit optical polarization to investigate laser coupling to the populations in equation (1). Starting from circular light, by 'detuning' the phase offset between the laser electric field components we can precisely examine the system as increasing energy is coupled into

the oscillatory mode, as  $|\langle \mathbf{f}_L \rangle - \mathbf{f}_L| > 0$ . Our method is as follows: two lasers are injected through the  $x = 0$  boundary, each linearly polarized in the opposite plane with normalized intensity  $a_0/\sqrt{2}$ . From this setup, precise control over the oscillatory electron energy is possible by tuning the relative offset between the phases of the two waves,  $\Delta\phi$  [rad]. In this notation,  $\Delta\phi = \pi/2$  corresponds to circular light and  $\Delta\phi = 0$  corresponds to linear light, with the total amplitude of the light equal to  $a_0$  for arbitrary  $\Delta\phi$ . We have checked that the  $\Delta\phi = 0$  simulations agree closely with simulations performed using a single linearly-polarized laser. This approach has an important experimental analog, as maintaining ideal polarization phases is challenging under realistic conditions.

Fig. 4 compares the analytic predictions to simulation results for various  $a_0, n_0$  configurations for  $\Delta\phi = \pi/2$  (circularly-polarized) light. (A,C,E) show the simulation results for the energy coupled into the oscillatory (red) and steady-state (blue) absorption modes. The cumulative particle energy is normalized to the total field energy injected into the simulation for an equivalent 'empty' run with no plasma,  $\int I_L dA dt$ . The simulation instantaneous particle energy flux is normalized to the attenuated injected energy flux density from the laser as noted in equation (32),  $(1 - \beta_p)I_L$ . We find that the proper normalization coefficients,

$$C_0 = (1 - \beta_p)I_L \quad (42)$$

$$C_1 = \int I_L dA dt \quad (43)$$

are essential so that measurements of the instantaneous coupling agree with measurements of the cumulative energy coupling, confirming equation (22). With this approach, we have checked that the full time-integrated photon energy passing through the simulation boundaries agrees with the total and instantaneous energy absorbed into particles.

We note that care must be taken in measuring the instantaneous reflection using light passing through the simulation boundaries, as the energy flux associated with the reflected photons undergoes both doppler red-shifting and dispersion over time, due to the additional distance  $dx = 2u_p dt$  traveled. Because  $I_L$  corresponds to the laser light reaching the overdense target surface, as noted in equation (30), care must also be taken in scenarios with large-scale underdense plasma regions.

Predictions from the model are overlaid on the simulation results in Fig. 4 (A,C,E), calculated using reflection data from the simulations at 30fs intervals. The model is seen to closely agree with the simulation data to within fractions of a percent. Plots (B,D,F)

show the corresponding front velocity  $\beta_p$  from the simulations and model, for the Wilks model (purple), Naumova model (black) and our model (red). The piston velocity from the simulation is measured using two methods: first, the location of the interface defined by  $n_i/n_0 = 1$  is tracked over time at 10fs intervals. The green curve represents the derivative of the front location over time, with oscillations in the piston velocity described in [13]. Second, we measure the doppler-shifting in the frequency of the  $1\omega_L$  light in the  $E_z$  transverse electric field passing through the simulation boundary. The relativistic piston velocity  $\beta_p$  is related to the frequency shift through  $\Delta f/f_0 = 1 - (1 - \beta_p)/(1 + \beta_p)$ . Blue dots on the curve represent the Fourier transformed simulation data at 100fs intervals, and are seen to be within one percent of the density front velocity metric. The analytic model predictions are seen to be within one percent of the simulation data across laser intensities. Plots (C-D) use  $a_0 = 20\sqrt{2}, n_0/n_{cr} = 20$  and show good agreement with results obtained in [13]. Plots (E-F) correspond to  $a_0 = 100, n_0/n_{cr} = 30$ , showing the steady-state interaction far below the relativistic critical density threshold[10]. The protons reflected from the piston in this simulation attain kinetic energy of  $\sim 100$  MeV.

Fig. 5 illustrates the effects of varying the laser polarization offset for the  $a_0 = 100, n_0/n_{cr} = 30, Z/A = 1$  plasma simulation, depicted for  $\Delta\phi = \pi/2$  in Fig. 4 (E-F). The electron and ion phase space from the simulation are depicted in the (Top) and (Middle) rows for  $\Delta\phi = \pi/2, 0.92$ . In the  $\Delta\phi = 0.92$  simulation, the piston structure is observed to reflect the background ions effectively even as 10% more energy is coupled into the oscillatory mode electrons, relative to the  $\Delta\phi = \pi/2$  simulation. Plot (Bottom Row) (A-B) show the model predictions for this case, showing agreement to within 5% in coupling efficiencies and in the piston velocity. Plot (Bottom) (C) shows the analytic curves for  $f_a^p$  (blue) and  $f_a^h$  (red) for  $a_0 = 100, n_0/n_{cr} = 30$ , as well as the light absorption limit indicated with red and blue dots. Results from the simulations are overlaid along the curves. From right-to-left, the colored  $\nabla$  markers represent simulation results for  $\Delta\phi = \pi/2, 0.95, 0.92, 0$ . As the polarization tends further towards linear, simulation results show a jump in the total energy absorbed by the plasma. This is due to the fact that the laser piston no longer fully reflects ions, allowing electrons to fall through the piston potential. Consistent with the assumptions underlying the model, accuracy falls beyond this point as additional effects such as shock acceleration of ions modify the partitioning of energy coupled into the plasma. The dynamics of these effects, recently reported on in detail[18], fall outside the scope of

this paper.

Due to the restricted set of accessible states in 1-D geometry, full linear polarization is seen to couple 47% of the laser energy into the target, relative to 37% for  $\Delta\phi = \pi/2$  and 41% for  $\Delta\phi = 0.92$ . These conversion efficiencies are high as ions in this interaction are accelerated relativistically, with the corresponding shock velocity scale  $\beta_0 = 0.3$ . Absorption decreases as  $\beta_0$  becomes smaller, with nonlinear dependencies given by equations (39-41).

Laser coupling into the oscillatory absorption mode is illustrated in Fig. 6 for the  $\beta_0 = 0.295, \Delta\phi = 0.92$  simulation. (A) depicts the density of exchange mediating electrons (red) and of ions (black) at two times, with the arrows indicating the dynamical position of the laser-plasma interface. The density of electrons coupled into the oscillatory mode,  $n_h$ , is calculated in the simulation as the subset of exchange-mediating electrons passing through the  $x = 100\mu\text{m}$  plane as shown in (B). The associated relative mass density  $\bar{\rho}_h \ll 1$  given by equation (36) is labeled on the right axis. (D) depicts the ensemble average Lorentz factors for the exchange-mediating electrons and for the hot electrons. Fig. 6 (C) compares simulation results to the analytical model. The dashed black line corresponds to equation (40) using the average reflection coefficient 0.61 from Fig. 5. The hot electron energy flux density  $d\mathcal{E}_h/(dA dt)$  is self-consistently calculated through a diagnostic in the simulation. The solid blue curve shows this quantity normalized to equation (22) using the constant laser intensity  $I_L$ . The ensemble average quantity  $\gamma_h$  and  $\bar{\rho}_h$  from the simulation are used to calculate the solid black curve, according to equation (34). The good agreement between the analytic model and the simulation results is illustrated in (C).

## IX. ASTROPHYSICAL APPLICATIONS

The results presented in this paper for the deposition of laser energy into hole punching ion and hot electron components are germane to topical astrophysical problems. Most notably, such conversion efficiencies are core unknowns in the study of astrophysical jets. There is a growing enthusiasm among astrophysicists for the paradigm that Poynting flux-dominated outflows in gamma-ray bursts (e.g. [19, 20]) and blazars (e.g. [21, 22] and references therein) drive their energization and dissipation at large distances from their central "engines". Most gamma-ray bursts (GRBs) are thought to emanate from powerful explosions of hypermassive stars located in distant galaxies in the early universe, at redshifts of around  $z = 1$  or larger

[23, 24]. A smaller number of so-called “short” bursts may be the result of neutron star–black hole mergers. The energy release of  $10^{51}$ – $10^{54}$  ergs is comparable to or somewhat higher than conventional supernovae in our Milky Way galaxy, but a key signature is that it drives a collimated, ultra-relativistic outflow (i.e., jet) with bulk Lorentz factors  $\Gamma$  in excess of several hundred [25, 26]. Blazars are also extragalactic jet sources, but generally nearer by and less luminous than GRBs, and with inferences of less extreme bulk motions ( $\Gamma \sim 3$ – $50$ ). They emanate from the environs of persistent supermassive black holes, exhibiting highly variable optical, X-ray [27] and gamma-ray emission, all the way up to a few TeV in photon energy. The variability in these wavebands can sometimes be as short as a few minutes, thereby indicating a compact physical scale of around  $10^{13}$  cm for the emission/activation zone. The rapid flaring is most easily explained by interpreting the jets in blazars as being pointed almost directly towards an observer; relativistic Doppler effects then drive the large amplitudes of the flux fluctuations. Optical polarization measurements (e.g. see [28] for 3C 279) suggest that synchrotron emission from somewhat coherent magnetic field regions is what is seen in blazars, and this is the prevailing paradigm for non-thermal GRB jet emission also.

A key element of our understanding of both gamma-ray bursts and blazars is that the activation/emission region is not located right near the central engine, but is some distance/time further out. For bursts, the zone near the explosion event is Thomson optically thick to gamma-rays, and most of the emission we see does not resemble a blackbody spectrum. Therefore the radiative dissipation must arise predominantly outside the photosphere that is expected early in the expanding flow, and typically must arise at distance of  $10^{15}$ – $10^{17}$  cm from the “hypernova” event. Similarly, blazars may become active only after their jets have been propagating for some time outside the black hole environs, an inference suggested by the optical polarimetry of synchrotron emission associated with gamma-ray flaring activity [28]. Accordingly, a core question for these topical sources is how is the energy transported out from the central region, and what is the most efficient means for doing so. It was realized long ago [23, 29] that pushing ions with the explosive force of a GRB progenitor star would lead to unreasonably large requirements for the energy of the explosion. This defined the so-called “baryon-loading” problem for GRB jets, and led to the preferred paradigm of electron-positron pair jets composed of much lighter particles that are more easily accelerated to bulk speeds with  $\Gamma > 100$ . The same is true for blazar jets. Yet what inhibits them

from radiating efficiently until large distances from the central engine? This conundrum has precipitated the class of electromagnetic driver models [19, 20], where Poynting flux dominates the inner outflow zone in an inert mode, and converts to bulk kinetic energy and dissipates only after a while, perhaps via magnetic reconnection, thereby activating the jet particles so that they radiate the non-thermal gamma-rays and X-rays that we detect. It must be remembered that prevailing ideas concerning jet launching and propagation mostly require the presence of magnetic fields to effect continued collimation [30, 31]. Imbuing the jet with a dominant electromagnetic component is an efficient means for propagating energy out from the central regions and delaying the onset of radiative dissipation.

Understanding the efficiency of conversion of direct electromagnetic energy to plasma kinetic and thermal energies is therefore an extremely desirable advance. Astrophysicists modeling jet sources need to comprehend at greater depth how the electromagnetic energy is reassigned to electrons and ions. Laser-driven plasma interaction and associated kinetics can therefore provide crucial insights into these astrophysical phenomena. This study and its results on laser light absorption is an important step in this direction. Formulating simple equations such as equation (40) to describe the ultimate kinematic apportionment of laser energy into hot electrons (efficient radiators) provides a first guide to how efficiently we think gamma-ray bursts and blazars can radiate if their outflows are mediated mostly by Poynting flux at early epochs in their expansion. Moreover, anticipating that down the line this study can address higher laser intensities, we can extend the focus to the relativistic flow speeds germane to bursts and blazars. This will then explore parameter regimes that precipitate rampant pair production, and therefore sample the domain of pair jets, perhaps the preferred picture for the later radiative phases of these highly variable astrophysical sources. An interesting potential future foray could be to explore multiple laser-plasma interaction sites corresponding an array of bulk flows, and these will in turn interact, forming collisionless shock zones, where charges will be energized and radiate the electromagnetic signals that we detect from GRBs and blazars.

## X. CONCLUSION

In conclusion, we have developed a more comprehensive model of ultraintense laser absorption, allowing the light to couple into both the hole punching and hot electron absorp-

tion modes in an energetically significant fashion for the first time. The fully-relativistic model has been derived for arbitrary overdense interaction densities and is insensitive to laser polarization assuming that bulk ions are swept up and fully reflected by the laser piston. Close agreement between the analytic model and particle-in-cell simulations has been demonstrated, justifying the assumptions underlying the kinematic approach.

Using this framework, we have obtained solutions for the particle distribution function moments that simultaneously satisfy energy and momentum conservation, i.e. the relativistically-correct hole punching velocity including the hot electrons, and the hot electron Lorentz factor. For the first time, analytic expressions for the conversion efficiencies into hole punching ions and into hot electrons have been derived. These results open the door to addressing a number of interesting ultraintense laser plasma applications in the future.

M. L. is grateful to Steve Libby for advice and stimulating conversations, and to he and Laurent Divol for their encouragement of continued research into basic laser plasmas. M. L. also thanks Tony Link for useful discussions regarding LSP.

This work was performed under the auspices of the U.S. Department of Energy by Lawrence Livermore National Laboratory under Contract DE-AC52-07NA27344.

- 
- [1] S. C. Wilks, W. L. Kruer, M. Tabak, and A. B. Langdon. Absorption of ultra-intense laser pulses. *Physical Review Letters*, 69(9):1383–1386, August 1992.
- [2] Victor Malka, Jérôme Faure, Yann A Gauduel, Erik Lefebvre, Antoine Rousse, and Kim Ta Phuoc. Principles and applications of compact laserplasma accelerators. *Nature Physics*, 4(6):447–453, June 2008.
- [3] M. Tabak, James Hammer, Michael E Glinsky, W. L. Kruer, S. C. Wilks, John Woodworth, E Michael Campbell, Michael D Perry, and Rodney J Mason. Ignition and high gain with ultrapowerful lasers. *Physics of Plasmas*, 1(May):1626–1634, 1994.
- [4] S.V Bulanov, T.Zh Esirkepov, V.S Khoroshkov, A.V Kuznetsov, and F Pegoraro. Oncological hadrontherapy with laser ion accelerators. *Physics Letters A*, 299(23):240 – 247, 2002.
- [5] M. Haines, M. Wei, F. Beg, and R. Stephens. Hot-Electron Temperature and Laser-Light Absorption in Fast Ignition. *Physical Review Letters*, 102(4):1–4, January 2009.
- [6] H. Chen, S. C. Wilks, James Bonlie, E. Liang, Jason Myatt, D. F. Price, D. D. Meyerhofer, and Peter Beiersdorfer. Relativistic Positron Creation Using Ultraintense Short Pulse Lasers. *Physical Review Letters*, 102(10):1–4, March 2009.
- [7] N. Naumova, T. Schlegel, V. Tikhonchuk, C. Labaune, I. Sokolov, and G. Mourou. Hole Boring in a DT Pellet and Fast-Ion Ignition with Ultraintense Laser Pulses. *Physical Review Letters*, 102(2):1–4, January 2009.
- [8] S. C. Wilks and W. L. Kruer. Absorption of ultrashort, ultra-intense laser light by solids and overdense plasmas. *IEEE Journal of Quantum Electronics*, 33(11):1954–1968, 1997.
- [9] Y. Ping, a. Kemp, L. Divol, M. Key, P. Patel, K. Akli, F. Beg, S. Chawla, C. Chen, R. Freeman, D. Hey, D. Higginson, L. Jarrott, G. Kemp, a. Link, H. McLean, H. Sawada, R. Stephens, D. Turnbull, B. Westover, and S. Wilks. Dynamics of Relativistic Laser-Plasma Interaction on Solid Targets. *Physical Review Letters*, 109(14):1–5, October 2012.
- [10] F Cattani, A Kim, D Anderson, and M Lisak. Threshold of induced transparency in the relativistic interaction of an electromagnetic wave with overdense plasmas. *Physical review. E, Statistical physics, plasmas, fluids, and related interdisciplinary topics*, 62(1 Pt B):1234–7, July 2000.
- [11] R. D. Hazeltine and S. M. Mahajan. Generalization of collisional fluid theory to long mean-

- free-path and relativistic motion. *Physics of Plasmas*, 9(8):3341, 2002.
- [12] W. L. Kruer and Kent Estabrook. JB heating by very intense laser light. *Physics of Fluids*, 28(1):430, 1985.
- [13] T Schlegel, N Naumova, V T Tikhonchuk, C Labaune, I V Sokolov, and G Mourou. Relativistic laser piston model: Ponderomotive ion acceleration in dense plasmas using ultraintense laser pulses. *Physics of Plasmas*, 16(8):083103, 2009.
- [14] a. P. L. Robinson. Production of high energy protons with hole-boring radiation pressure acceleration. *Physics of Plasmas*, 18(5):056701, 2011.
- [15] L. a. Cottrill, a. B. Langdon, B. F. Lasinski, S. M. Lund, K. Molvig, M. Tabak, R. P. J. Town, and E. a. Williams. Kinetic and collisional effects on the linear evolution of fast ignition relevant beam instabilities. *Physics of Plasmas*, 15(8):082108, 2008.
- [16] Hiroyuki Daido, Mamiko Nishiuchi, and Alexander S Pirozhkov. Review of laser-driven ion sources and their applications. *Reports on progress in physics. Physical Society (Great Britain)*, 75(5):056401, May 2012.
- [17] D.R. Welch, D.V. Rose, R.E. Clark, T.C. Genoni, and T.P. Hughes. Implementation of a non-iterative implicit electromagnetic field solver for dense plasma simulation. *Computer Physics Communications*, 164(1-3):183–188, December 2004.
- [18] F. Fiuza, A. Stockem, E. Boella, R. Fonseca, L. Silva, D. Haberberger, S. Tochitsky, C. Gong, W. Mori, and C. Joshi. Laser-Driven Shock Acceleration of Monoenergetic Ion Beams. *Physical Review Letters*, 109(21):215001, November 2012.
- [19] M. Lyutikov and R. D. Blandford. Electromagnetic outflows and grbs. *Astron. Soc. Pacific Conf. Series*, 312(449), 2004.
- [20] B. Zhang & A. Pe’er. Evidence of an initially magnetically dominated outflow in grb 080916c. *Astrophys. J.*, 700(L65), 2009.
- [21] T. Chiueh & M. C. Begelman Z.-Y. Li. Electromagnetically driven relativistic jets - a class of self-similar solutions. *Astrophys. J.*, 394(459), 1992.
- [22] G. M. Madejski & J.-P. Lasota M. Sikora, M. C. Begelman. Are quasar jets dominated by poynting flux? *Astrophys. J.*, 625(72), 2005.
- [23] T. Piran. Gamma-ray bursts and the fireball model. *Phys. Rep.*, 314(575), 1999.
- [24] P. Mészáros. Theories of gamma-ray bursts. *Ann. Rev. Astron. Astr.*, 40(137), 2002.
- [25] M. G. Baring. Temporal evolution of pair attenuation signatures in gamma-ray burst spectra.

- Astrophys. J.*, 650(1004), 2006.
- [26] A. A. Abdo et al. *Fermi* observations of high-energy gamma-ray emission from grb 080916c. *Science*, 323(1688), 2009.
- [27] D. E. Harris & H. Krawczynski. X-ray emission from extragalactic jets. *Ann. Rev. Astron. Astr.*, 44(463), 2006.
- [28] A. A. Abdo et al. A change in the optical polarization associated with a gamma-ray flare in the blazar 3c279. *Nature*, 463(919), 2010.
- [29] A. Shemi & T. Piran. The appearance of cosmic fireballs. *Astrophys. J.*, 365(L55), 1990.
- [30] Y. Mizuno, P. Hardee, and K. I. Nishikawa. Relativistic mhd simulations of relativistic jets with raishin. *Astrophys. J.*, 662(835), 2007.
- [31] J. C. McKinney & R. D. Blandford. Stability of relativistic jets from rotating, accreting black holes via fully three-dimensional magnetohydrodynamic simulations. *Mon. Notices R. Astron. Soc.*, 394(L126), 2009.

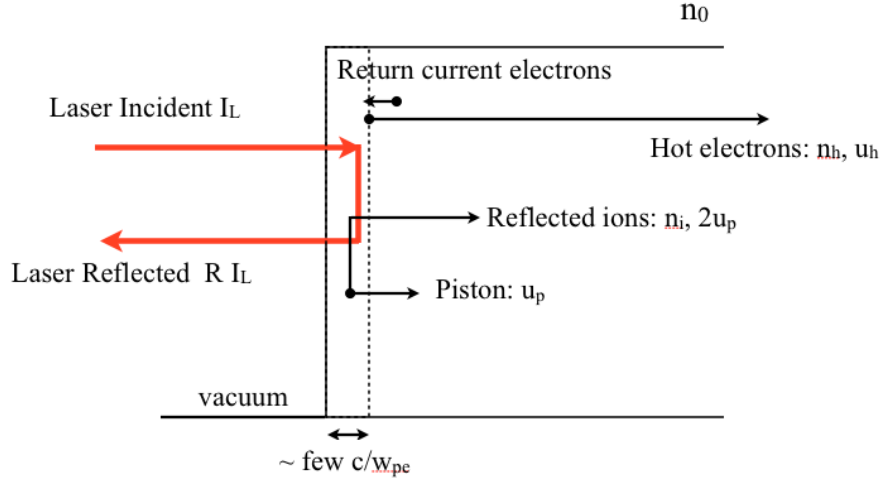


FIG. 1: Schematic depicting the laser plasma coupling in the interaction region with  $n_0 = n_e = n_i/Z$  where  $Z$  is the ion charge state. The laser piston boundary is represented by the dashed line. The bulk ions reflected from the piston and the hot electron beam represent the energetically significant particle fluxes.

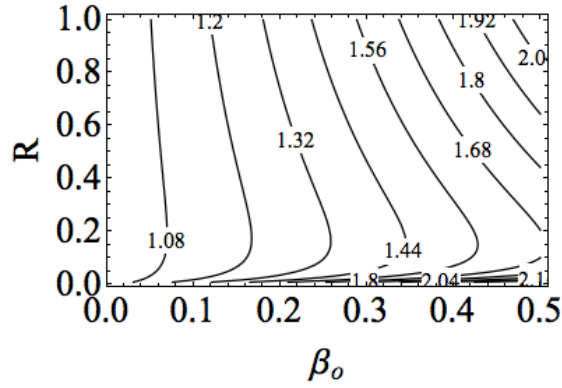


FIG. 2: Contours of the  $O(1)$  term from equation (38).

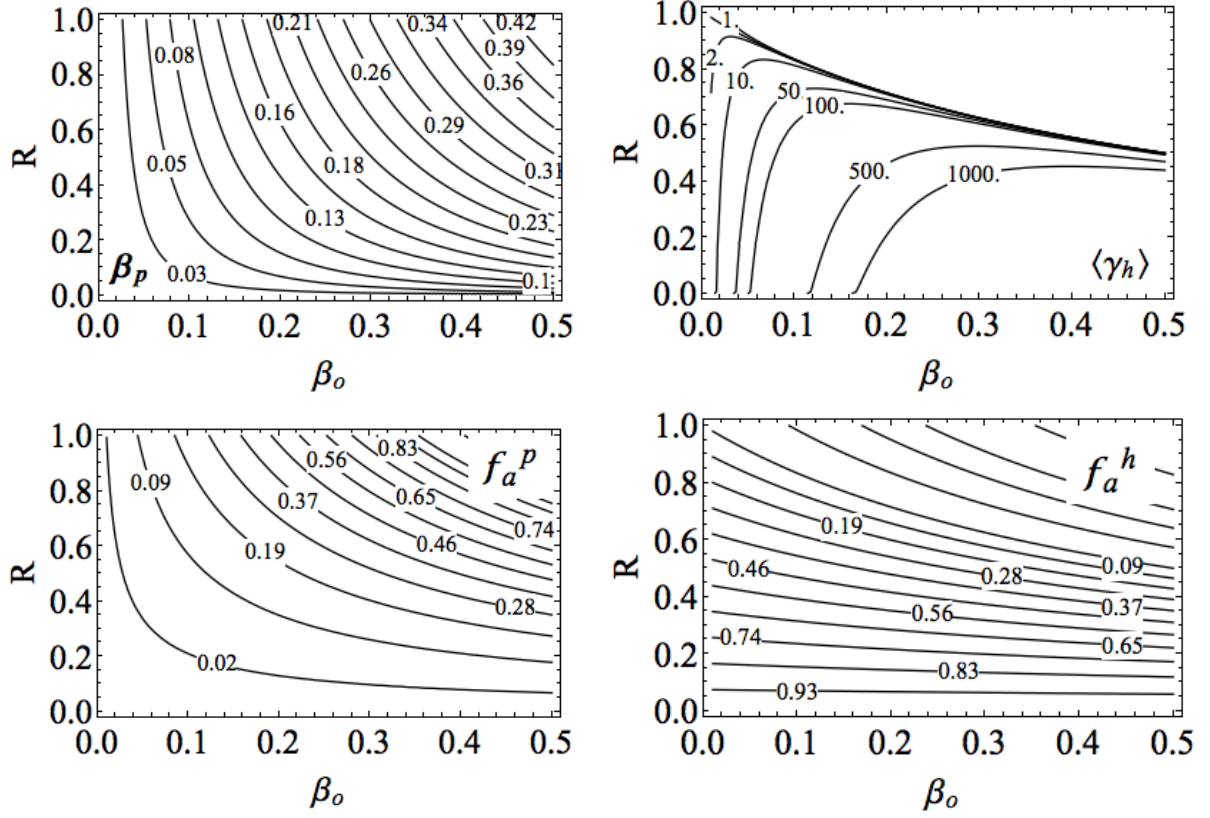


FIG. 3: (A-B) Analytic solutions satisfying energy and momentum conservation with the laser,  $\{\gamma_h, \beta_p\}$ . (C-D) Contours of the laser conversion efficiencies into each absorption mode.

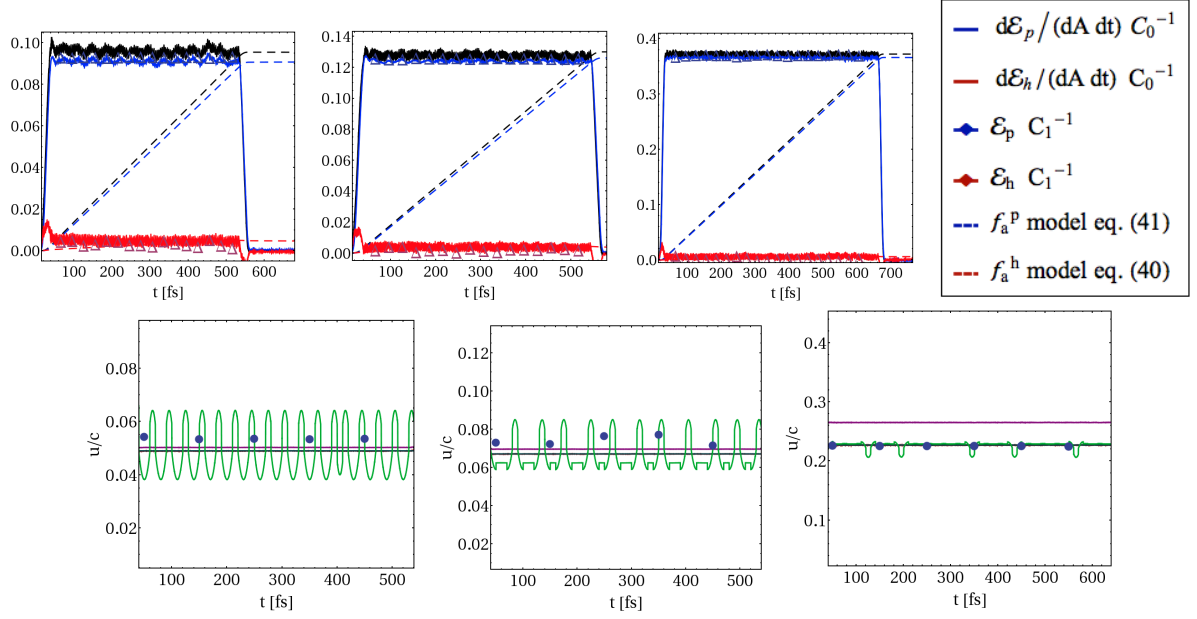


FIG. 4: (Top) Laser absorption into hole punching ions and hot electrons, simulation and analytic model for  $\Delta\phi = \pi/2$  (Left-to-Right)  $a_0 = 32, n_0/n_{cr} = 50$  ( $\beta_0 = 0.073$ ),  $a_0 = 20\sqrt{2}, n_0/n_{cr} = 20$  ( $\beta_0 = 0.102$ ), and  $a_0 = 100, n_0/n_{cr} = 30$  ( $\beta_0 = 0.295$ ). (Middle) Piston velocity  $\beta_p$  from the simulations and analytic model. Simulation data from FFT is indicated by blue dots and simulation data obtained by tracking the critical surface over time is plotted in green.

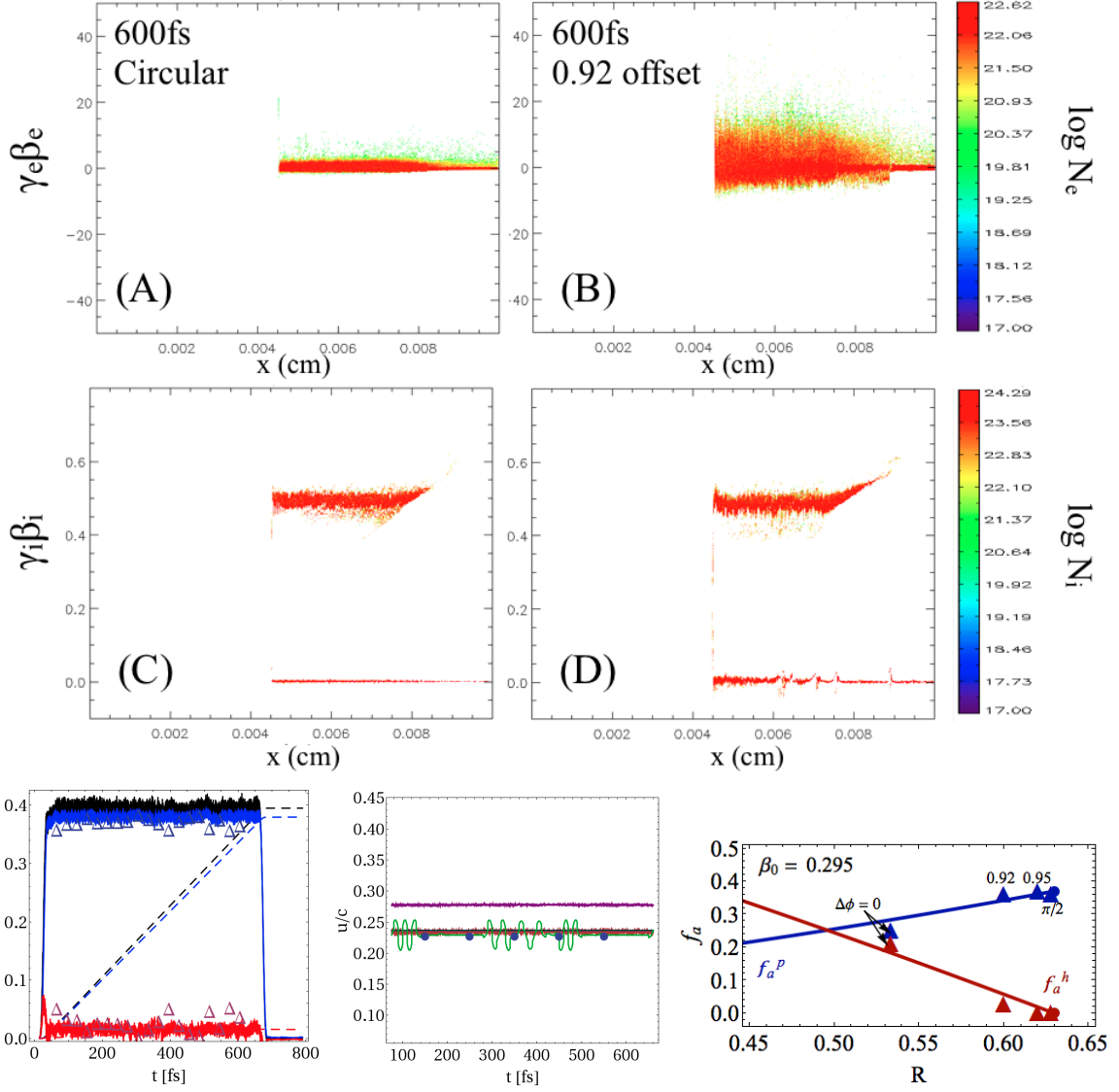


FIG. 5: Comparison of simulation and model as the laser polarization phase offsets vary from circular towards linear for the  $a_0 = 100, n_0/n_{cr} = 30, Z/A = 1$  plasma simulation, corresponding to  $\beta_0 = 0.295$ . (A-B) Electron phase plots for  $\Delta\phi$  [rad] =  $\pi/2, 0.92$ . (C-D) Ion phase space plots corresponding to above. (Bottom Row, Left and Middle) Simulation and model results overlaid for the  $\Delta\phi = 0.92$  simulation. (Bottom Right) Comparison of laser coupling to model.

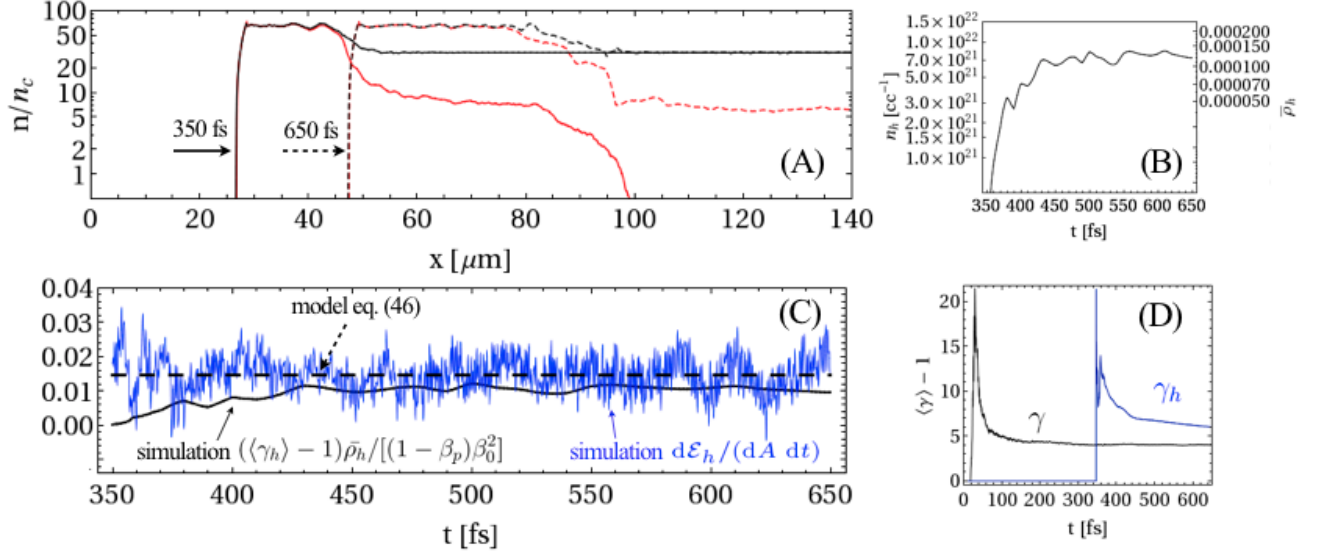


FIG. 6: Coupling to the oscillatory component of the laser ponderomotive force for the  $\beta_0 = 0.295$ ,  $\Delta\phi = 0.92$  simulation. (A) Number density of exchange-mediating electrons (red) and of ions (black). Arrows indicate the position of the laser-plasma interface. (B) Hot electron density  $n_h$  and  $\bar{\rho}_h$ . (C) Comparison of hot electron absorption from the simulation to the analytic model. (D) Ensemble average Lorentz factors (see text).